RSC Advances



This is an *Accepted Manuscript*, which has been through the Royal Society of Chemistry peer review process and has been accepted for publication.

Accepted Manuscripts are published online shortly after acceptance, before technical editing, formatting and proof reading. Using this free service, authors can make their results available to the community, in citable form, before we publish the edited article. This Accepted Manuscript will be replaced by the edited, formatted and paginated article as soon as this is available.

You can find more information about *Accepted Manuscripts* in the **Information for Authors**.

Please note that technical editing may introduce minor changes to the text and/or graphics, which may alter content. The journal's standard <u>Terms & Conditions</u> and the <u>Ethical guidelines</u> still apply. In no event shall the Royal Society of Chemistry be held responsible for any errors or omissions in this *Accepted Manuscript* or any consequences arising from the use of any information it contains.



ROYAL SOCIETY OF CHEMISTRY

Journal Name

ARTICLE

Influence of Facets and Heterojunctions in Photoactive Bismuth Oxylodide

Received 00th January 20xx, Accepted 00th January 20xx

DOI: 10.1039/x0xx00000x

www.rsc.org/

Aijuan Han,^{a,b} Jiulong Sun,^{a,b} Xuanhao Lin,^a Cheng-Hui Yuan,^a Gaik Khuan Chuah*^a and Stephan Jaenicke*^a

The role of facetted crystalline nanosheets and heterojunctions in bismuth oxyiodide composites for the photodegradation of phenolic compounds is investigated. Single-crystalline nanosheets with either $\{001\}$ or $\{110\}$ planes as the domina facets were formed by tuning the pH during synthesis. The $\{001\}$ -facetted BiOI consisted of large crystallites with low surface areas in contrast to the thinner and smaller $\{110\}$ -facetted platelets. The specific activity per m^2 for the photodegradation of p-cresol was ~ 5 times higher over the $\{001\}$ than over the $\{110\}$ -facetted BiOI which can be correlated to the stronger adsorption of the substrate at the oxygen-rich $\{001\}$ surface. However, the low surface area of $\{10\}$ of $\{110\}$ -facetted BiOI at $\{110\}$

Introduction

The activity of a photocatalyst depends on a number of factors including band gap and surface area. While the width of the band gap affects the optical absorption characteristics, the absolute band position (referenced against the Fermi level or the potential of the normal hydrogen electrode) determines the reduction and oxidation abilities. 1 A higher surface area is usually beneficial as more active surface sites are available.² However, for a nonporous material, a higher surface area means smaller particle size which in turn could increase the rate of surface electron/hole recombination, thus offsetting the benefits of the high surface area. Hence there is an optimum particle size for photocatalysts.3 Furthermore, different crystal facets possess particular electronic and geometric structures that offer distinctive photocatalytic activities. Anatase titania with {001} facets has been found to be more reactive than titania with {101} facets due to differences in surface energy. 4-6 Jiang et al. reported that (SCNs) single-crystalline nanosheets of **BiOCI** with

predominantly exposed {001} facets exhibited high activity for the direct semiconductor photoexcitation leading to pollutant degradation under UV light, while the material with exposed {010} facets had higher activity for the indirect dye-sensitized photodegradation under visible light. Hence, the facet-controlled fabrication of single-crystalline photocatalystalintroduces another degree of freedom in the design of photocatalysts. Photocatalysts. Photocatalysts.

BiOI has a tetragonal PbFCI (matlockite) structure where $[Bi_2O_2]$ slabs are interleaved between double layers of iodine ions (Fig. 1a). The electrons in the 5s orbital of the iodine ions are easily excited, so that the band gap of BiOI is only $^{\sim}$ 1.8 eV. Hence, it can utilize a large proportion of the visible light spectrum. BiOI in different morphologies such as nanoparticles, 13,14 nanobelts, 15 nanoplates, 16,17 and 3D microspheres $^{18\cdot21}$ has been reported as photocatalyst for the decomposition of various organic pollutants such as Rhodamine B, methyl orange, and phenol. Studies on BiOI single crystalline nanosheets prepared by annealing BiI₃ in $^{-10}$ showed that the {001} facets are most reactive. 22

In view of these reports, we were interested in the factors that influence the photoactivity of BiOI such as morpholog, surface area and heterojunctions. We adjusted the synthesis pH to direct the facet formation in BiOI, similar to that reported for BiOCI.⁷ The density of oxygen atoms in the (00) and (110) planes differs, being 6.27 and 1.94 atoms/nm², respectively (Fig. 1). Under acidic conditions, H⁺ will | adsorbed more strongly on the O-terminated (001) than on the

^a-Department of Chemistry, National University of Singapore, 3 Science Drive, Singapore 117543, Singapore.

E-mail: chmcgk@nus.edu.sg Tel: +65 6516 2839 Fax: +65 6779 1691 E-mail: chmsj@nus.edu.sg Tel: +65 6516 2918 Fax: +65 67791691

b. NUS Environmental Research Institute, National University of Singapore, 5A Engineering Drive 1, #02-01, Singapore 117411, Singapore.

[†] Footnotes relating to the title and/or authors should appear here.
Electronic Supplementary Information (ESI) available: [details of any supplementary information available should be included here]. See DOI: 10.1039/x0xx00000x

ARTICLE Journal Name

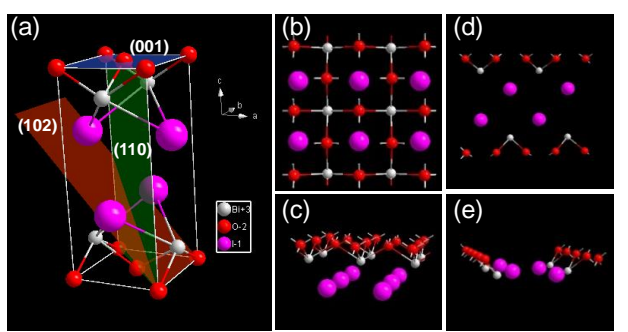


Fig. 1 (a) Crystal structure of BiOI, (b, d) top and (c, e) side views of the atomic arrangement in the (001) and (110) facets.

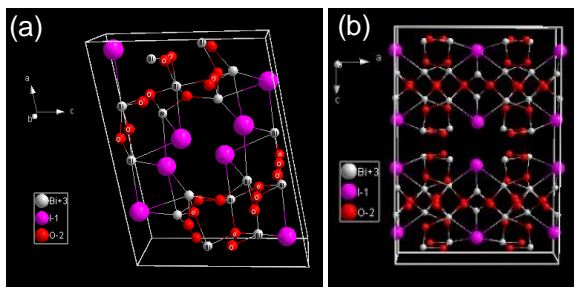


Fig. 2 Crystal structure of (a) $Bi_4O_5I_2$ and (b) α - Bi_5O_7I .

(110) surface. Consequently, growth in the [001] direction is hindered, leading to predominance of (001) facetted planes. At higher pH, this hindrance is reduced due to the lower H⁺ concentration, and other slow growing planes become predominant.

To form heterojunctioned composites, we took advantage of the fact that the iodine atoms in the BiOI structure can be easily replaced by oxygen atoms upon thermal treatment, resulting in various oxygen-rich bismuth oxyiodides, namely, $Bi_4O_5I_2$, $Bi_7O_9I_3$, and α - and β - $Bi_5O_7I.^{23-28}$ These bismuth oxyiodides share similar layered [BiO]+ structures but differ in the halogen content of the sandwich layer. In Bi₄O₅I₂, [BiO]⁺ layers (labelled with element name in Fig. 2a) run parallel to $(10\overline{1})$ with $[BiO_2]^-$ chains parallel to [010] attached on both sides. The [Bi₄O₅]²⁺ layers formed are separated from each other by layers of halogen ions. In $\alpha\text{-Bi}_5O_7I$, $[Bi_2O_2]^{2+}$ sheets aligned parallel to (001) are mutually connected by folded 1dimensional [Bi₄O₈]⁴⁻ ribbons with axes parallel to [010] and oriented parallel to (100) (Fig. 2b). We envision that the similarity of the crystal structures of the various bismuth oxyiodides should enable the formation of intimate junctions between the band structures in the crystalline domains in the $Bi_xO_yI_z$ composites, which at the right energy levels should facilitate electron-hole separation.

2. Experimental

2.1 Preparation of BiOI

Typically, 10 mmol of KI in 6 ml deionized water was added with stirring to a solution with 2 mmol of $Bi(NO_3)_3 \cdot 5H_2O$ in 21 ml deionized water, acidified with 1.4 ml glacial acetic acid. The required amount of 1 M NaOH solution was added to adjust the pH of the solution to x (x = 3, 4, 5, 6, 7, 8). After

stirring for 30 min, the solution was poured into a 40 ml Teflon-lined stainless steel autoclave and kept at 160 °C for 2 'under autogenous pressure. The resulting precipitate was collected by centrifugation, washed with absolute ethanol, and dried in an oven at 80 °C overnight. The product obtained w s denoted as BiOl-pHx. The pH of the suspension without adding any NaOH solution was 2.3, therefore this sample was denoted as BiOl-pH2.3.

2.2 Synthesis of bismuth oxylodide heterojunctions

The as-prepared BiOI-pH6 was calcined at 300 to 400 °C in air (1-5 h, 1 °C/min ramp) using a Nabertherm oven. The products obtained are denoted as BiOI-pH6-y-z where y represents the calcination temperature and z denotes the calcination time.

2.3 Characterization

Powder X-ray diffraction patterns were measured with Siemens D5005 diffractometer using Cu K_{α} radiation for $\overline{2\theta}$ from 5 - 80° at 0.02°/s and a dwell time of 1 s/step. Nitrogco adsorption and desorption isotherms were obtained at -196 °C using a TriStar 3000 Micromeritics porosimeter. The specific surface area was calculated using the BET (Brunauer-Emmett-Teller) equation. Scanning electron microscopy (SEM) war performed on a JEOL JSM-6701F SEM (field-emission) microscope with 5 kV electron beam energy. The sample was spread on a graphite adhesive tape and coated with ~ 2 nm Pt. Transmission electron micrographs were obtained with a JEOL 3010 operated at 200 kV. Thermogravimetric measurements were carried out using a TA Instruments SDT 2960 simultaneous DTA-TGA. Diffuse reflectance spectra were measured with Shimadzu UV-2450 **UV-Visible** spectrophotometer.

2.4 Photocatalytic activity

A suspension of 0.10 g photocatalyst in 100 ml of an aqueous solution of p-cresol (24 ppm) was magnetically stirred for 1 h to establish an adsorption-desorption equilibrium. An aliquot was removed to determine the p-cresol concentration in the solution before irradiation by a 22 W fluorescent lamp (3.3 x 1016 photons/s), placed 1 cm at the side of reactor. After specific time intervals, 2 ml aliquots were withdrawn and centrifuged at 6000 rpm for 5 min to remove any suspended particles. The concentration of p-cresol was determined from the absorption band at λ $^{\sim}$ 277.5 nm using a UV-vis spectrophotometer (Shimadzu, UV-1601). The degradation efficiency was calculated as: DE = 100 % \times (C_o - C)/C_o, where \bigcup_{c} is the concentration of p-cresol after equilibration in the dark, and C is the p-cresol concentration at time t. Photoactivity tests for other phenolic substrates were also carried out at 24 ppm concentration. The used catalyst was recovered by centrifugation, washed with deionized water, recalcines at 300 °C for 1 h and tested in further runs. To test the influence of other ions, the activity was also evaluated in the presence of 1 mM ammonium nitrate and sodium chlorid :. The total organic carbon (TOC) was measured with a Shimadzu TOC-VWS Total Organic Carbon Analyzer.

ARTICLE Journal Name

To detect intermediates of the p-cresol degradation, 20 ml of a p-cresol solution with concentration of 2.4 g/L was irradiated for 19 h in the presence of 0.4 g BiOI-pH6-350-3 under the same lamp. Aliquots were removed at different time intervals and analyzed on a Dionex Ultimate 3000 RSLC system coupled to an AmaZon X system (LC/MS). The column was a Luna C18, and atmospheric pressure chemical ionization (APCI) was used with full scan for negative ions from 70 to 500 amu. The mobile phase was 30 vol. % acetonitrile in water.

The nature of the active species was determined by investigating the photocatalytic degradation of p-cresol in the presence of various scavengers, i.e., K₂C₂O₄, t-butanol and KBrO₃. The procedure was the same as in the activity test except that a five-fold molar excess (relative to p-cresol) of the scavenger was added together with the photocatalyst. The presence of •OH radicals was deduced by trapping with terephthalic acid. Terephthalic acid itself does not fluoresce, but upon reaction with •OH radicals, 2-hydroxyterephthalic acid is formed which has a broad emission band with maximum at 425 nm. About 0.1 g of the photocatalyst was added to a 200 ml solution containing terephthalic acid (16.6 mg) in 2 mM NaOH. After irradiation with the 22 W fluorescent lamp, aliquots were removed at 30 min interval, centrifuged and the fluorescent emission spectrum of the solution was measured by a Gilden FluoroSNS-fluorimeter using an excitation wavelength of 315 nm.

3. Result and discussion

3.1 Characterization of BiOI synthesized at different pH

The x-ray diffractograms of BiOI synthesized between pH 2.3 to 7 were purely tetragonal (JCPDS 10-0045) (Fig. 3). Bismuth oxyiodide formed at pH 2.3 had diffraction peaks with high intensity especially those of the (00n) planes. The intensity of the (00n) peaks fell drastically in samples synthesized at higher pH but the (102) and (110) peak intensities remained unchanged. For pH 5 - 8, the (110) peak intensity was increased relative to the (102), indicating a predominance of this facet. The sample synthesized at pH 8 contained BiOI as well as $Bi_4O_5I_2$. The latter was identified from peaks at 2θ ~ 8.6° and 28.6° (JCPDS 12-1474). At this high pH, $Bi_4O_5I_2$ can form by the partial substitution of I $^-$ by OH $^-$ (4BiOI + 2OH $^ \rightarrow$ $Bi_4O_5I_2 + 2I^- + H_2O$).

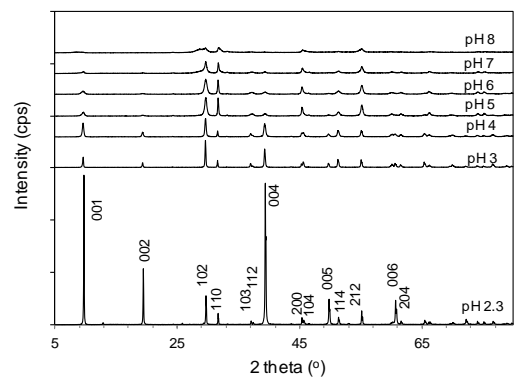


Fig. 3 X-ray diffraction patterns of BiOI samples prepared at different pH.

Table 1. Physical properties of BiOI samples synthesized at different pH

		XRD		Surf. Area	Eg
рН	(001)/(102)	(110)/(102)	Crys. size	(m ² g ⁻¹)	(eV)
			(nm)		
2.3	3.52	0.31	126	0.65	1.72
3	0.39	0.20	60.1	2.03	1.84
4	0.18	0.18	36.9	3.98	1.86
5	0.24	0.43	25.7	9.81	1.88
6	0.24	0.46	20.3	15.3	1.90
7	0.13	0.47	16.2	19.1	1.92
8	0.04	0.58	-	23.9	1.94

The crystallite size was calculated from the width of the (001) peak using the Scherer equation (Table 1). The crystallite size decreased from 126 to 16 nm as the synthesis pH rose from 2.3 to 7. This can be attributed to the decreasing solubility of BiOI with pH so that upon mixing of the reactant, precipitation occurs more rapidly and smaller crystallites form

Scanning electron microscopy (SEM) showed that irrespective of the synthesis pH, all the BiOI samples had plate-like morphology (Fig. 4). With increasing pH, the lamellae became smaller and thinner (Table 1). This change in morphology is reflected by an increase of surface area and the decrease in x-ray peak intensity. BiOI synthesized between pt 2.3 to 4 had surface areas of 0.65 to 3.98 m² g⁻¹ while materials synthesized at pH 5 to 8 had surface areas of 9.8 to 23.9 m² g⁻¹. The {001} facets were dominant in the transmission electron micrographs of BiOI synthesized below pH 4. For BiOI-pH2.3, lattice fringes with an interplanar spacing of 0.282 nm corresponding to the {110} atomic planes could be seen (Fig. 5). The sharp spots in the selected-area electron diffraction (SAED) pattern indicate the single crystalline nature. The labelled angle of 45° corresponds to that between the (110) and (200) planes for the tetragonal symmetry group, thus indexing the diffraction spots to the [001] zone axis. Therefore, the bottom and top surfaces of the BiOI-pH2.3 sample can be assigned to the {001} facets, which agrees well with the observed reflexes in XRD.

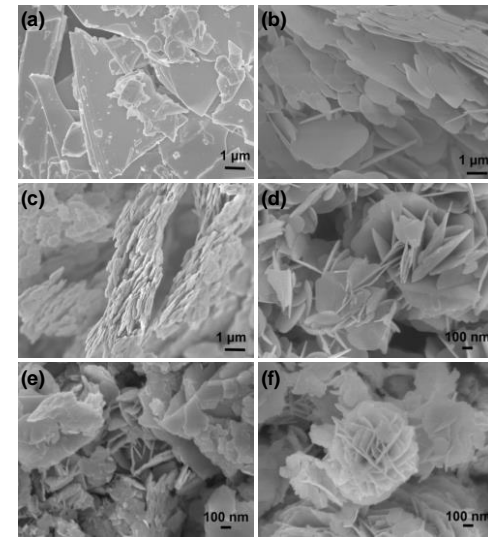


Fig. 4 SEM images of (a) BiOI-pH2.3, (b) BiOI-pH3, (c) BiOI-pH4, (d) BiOI-pH6 (e) BiOI-pH7, and (f) BiOI-pH8.

ARTICLE Journal Name

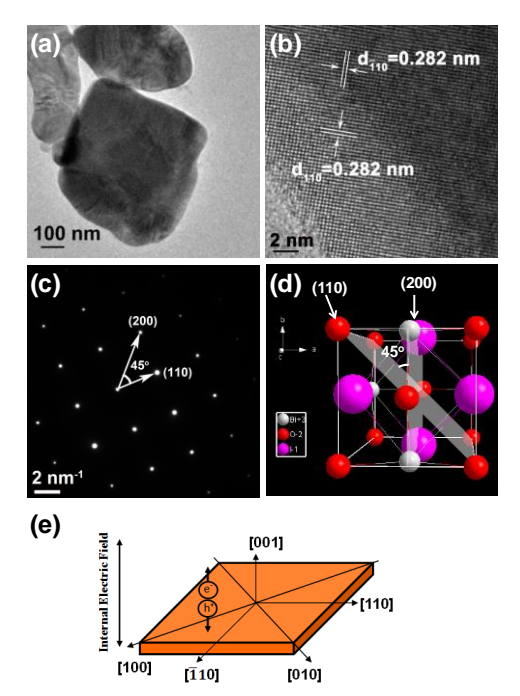


Fig. 5 (a) TEM image, (b) HR-TEM image, (c) SAED pattern, (d) top view of the (001) facet and (e) crystallographic directions for BiOl-pH2.3 SCN.

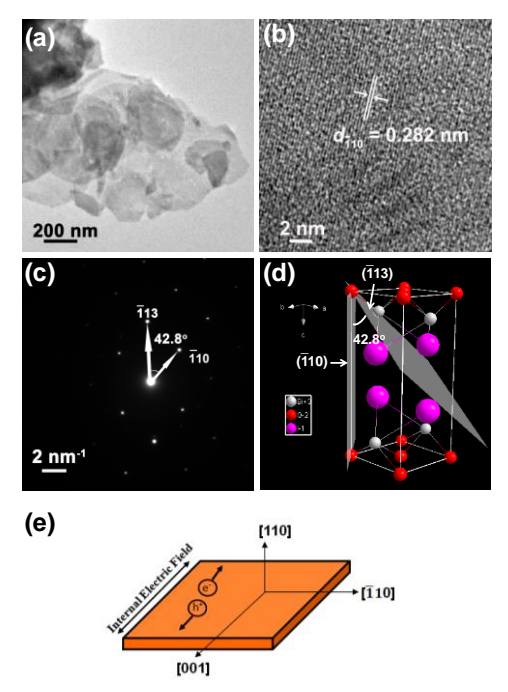


Fig. 6 (a) TEM image, (b) HR-TEM image, (c) SAED pattern, (d) top view of the (110) facet and (e) crystallographic directions for BiOl-pH6 SCN.

In contrast, the SAED pattern for BiOI synthesized at a higher pH of 6 shows the angle between the diffraction spots to be 42.8° (Fig. 6). This value corresponds to the angle between the ($\overline{1}13$) and ($\overline{1}10$) planes. The set of diffraction spots can therefore be indexed as the [110] zone axis of tetragonal BiOI so that the exposed facets are identified as those of {110}. Hence, by varying the pH during synthesis, it is possible to change the dominant exposed facets from (001) to (110).

The samples absorb in the visible range up to 670 nm (Fig. S1). The band gap energy was estimated from the intercept c'a $(F(R_\infty)\cdot h\nu)^{1/\eta}$ versus $h\nu$ plot, where $F(R_\infty)=(1-R_\infty)^2/2R_\infty$, $R_\infty=$ the reflectance of the sample using BaSO4 as a reference, ν = light frequency, E_g = band-gap energy, and η = 2 for an indire t transition. 29 The band gap increased slightly from 1.72 to 1.94 eV with higher pH during synthesis (Table 1). This increase is reflected by a change from dark red in BiOI-pH2.3 to orange for BiOI-pH8 (Fig. S2).

3.2 Photocatalytic activity of BiOI with different exposed facets

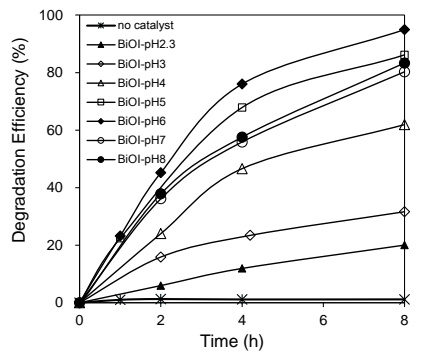
The photocatalytic activity of BiOI synthesized at different pH was assessed using p-cresol (CH₃(C₆H₄)OH) as a model pollutant. In the absence of the photocatalyst, there was almost no degradation of p-cresol under visible light irradiation (Fig. 7). The degradation efficiency can be correlated with the pH during synthesis: it increased to a maximum at pH 6 before decreasing with higher pH. However, BiOI synthesized at pH i and 8 were significantly more active than the materials prepared at acidic pH. Because the photodegradation norma"... takes place at the surface of the catalyst, surface structure and surface area will significantly influence the photoactivity. Pseudo first-order kinetics were applied to p-creso degradation according to the equation: $ln(C_0/C) = kt$ where k = 1the pseudo-first-order rate constant (Fig. S3). The rate constant was normalized to the catalyst weight (k_W) as well as the surface area (k_{SA}) to allow for a comparison of the activity

Interestingly, $k_{\rm W}$ and $k_{\rm SA}$ show different trends for BiOI synthesized at different pH. The rate constant per gram catalyst, k_W , increased 13-fold from 0.28 h⁻¹ g⁻¹ at pH 2.3 tc 3.65 h⁻¹ g⁻¹ at pH 6 before decreasing to ~ 2.1 h⁻¹ g⁻¹ for yet higher pH. On the other hand, the rate constant normalized surface area, k_{SA} , decreased from 0.43 h⁻¹ m⁻² at pH 2.3 to 0.09 h-1 m-2 at pH 8, showing that the intrinsic activity was higher for the {001}-dominated facets. To obtain an insight into the facet-dependent photocatalytic activity, we examined the adsorption capacities of p-cresol on the BiOI samples (Table 2). The samples formed at low pH with dominant {001} facets adsorb $0.33 - 0.44 \text{ mg } p\text{-cresol m}^{-2}$ as compared to only 0.02 - 0.04 mg0.06 mg m⁻² for materials formed at pH 5 - 8. The former values correspond to a complete monolayer based on an area of 0.385 nm² for the p-cresol molecule, as obtained from the density of the liquid assuming close packing of spherical molecules. The preferential surface coverage can be attributed to the high density of oxygen atoms at the {001} planes which favours the adsorption of p-cresol through hydrogen bonding with its hydroxyl group. The layered structure of BiOI leads to a permanent dipole between the [Bi₂O₂]²⁺ and I⁻ slabs, resulting in the generation of an internal electric field. Photon absorption creates an electron-hole pair in the bulk of the crystal. The electron-hole pairs are separated under the influence of this internal electric field. Because this internal field is perpendicular to the exposed facets in the {001}oriented crystals (Fig. 5e) but parallel in the {110}-facetted samples (Fig. 6e), the field supports diffusion of charges to the

Journal Name

surface along the shortest crystal dimension in the {001}-

dominant sample, leading to the higher k_{SA} .



 $\textbf{Fig. 7} \ \textbf{Photocatalytic activity of BiOI for } \textit{p-} \textbf{cresol degradation under visible light}.$

Table 2. Rate constant and p-cresol adsorption over BiOI prepared at different pH

рН	kw (h ⁻¹ g ⁻¹)	k _{SA} (h ⁻¹ m ⁻²)	C _{ads} (mg m ⁻²)
2.3	0.28	0.43	0.44
3	0.68	0.33	0.33
4	1.25	0.31	0.30
5	2.55	0.26	0.06
6	3.65	0.24	0.05
7	2.05	0.11	0.03
8	2.23	0.09	0.02

3.3 Formation of heterojunctioned composites

Although the intrinsic photoactivity of the {110}-dominant BiOI-pH6 was only about half that of the {001}-facetted BiOIpH2.3, it had a much higher surface area, 15.3 vs $0.65\ m^2\ g^{-1}$. This more than compensates for the photoactivity when used on an equal weight basis. We investigated whether calcination could further improve the activity. BiOI is stable up to 300 °C, whereupon it slowly transforms into Bi₄O₅I₂ (JCPDS 12-1474) with loss of iodine (Fig. S4). After calcination at 300 °C for 1 h, the diffraction peaks were shifted to smaller 2θ and broadened (Figs. 8 and S5). The peaks at 27.4° and 31.6° can be treated as characteristic peaks for BiOI and Bi₄O₅I₂, respectively. From the peak areas, the proportion of Bi₄O₅I₂/BiOI was 55:45 (Table 3). Composition changes calculated from the weight losses measured thermogravimetry gave Bi₄O₅I₂/BiOI of 59:41, in good agreement with the XRD results. An increase in the treatment temperature to 350 °C resulted in a shift of the diffraction lines to even smaller 2θ , where the diffraction pattern indicated the presence of a new phase, Bi₇O₉I₃. This is again corroborated by the weight loss upon heating the sample from 100 to 850 °C (Fig. S4). The measured weight loss of 17.7 % agrees closely with that calculated for the transformation of Bi₇O₉I₃ to Bi₂O₃ (17.9 %). Hence, it can be concluded that BiOI-pH6-350-1 is pure Bi₇O₉I₃. Extending the heating time at this temperature to 3 h resulted in the appearance of another bismuth oxyiodide compound, α-Bi₅O₇I (JCPDS 40-0548) which coexisted with $Bi_7O_9I_3$. From the peak areas, the proportion of $Bi_7O_9I_3/\alpha$ - Bi_5O_7I was 35:65 (Table 3). The proportion of α -Bi₅O₇I increased to

74:26 when the heating time was extended to 5 h. After treatment at an even higher temperature (400 °C), only the pure α-Bi₅O₇I phase was observed (Fig. 8). Thus, by varying the heating time at 350 °C, compositions with different proportions of Bi₇O₉I₃ and α-Bi₅O₇I could be formed. Scanning electron micrographs revealed that the plate-like morphology of the material was not affected by the calcination (Fig. S6).

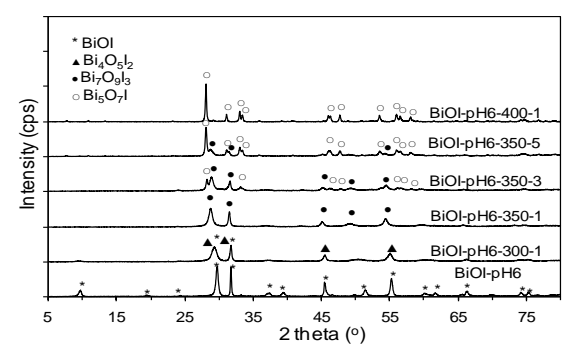


Fig. 8 X-ray diffractograms of as-synthesized and calcined BiOI-pH6 samples.

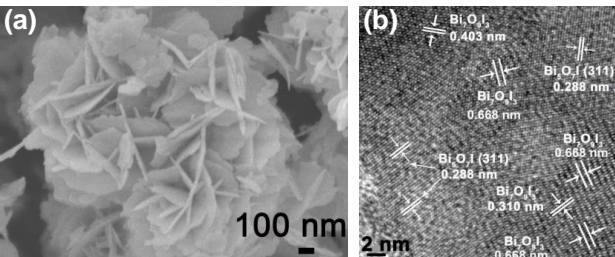


Fig. 9 (a) FESEM and (b) HRTEM images of BiOI-pH6-350-3.

Four distinct lattice spacings are observed in the HRTEM of BiOI-pH6-350-3 (Fig. 9b). The lattice spacing of 0.288 nm can be uniquely assigned to the (311) lattice plane of α-Bi₅O₇I while the others at 0.310, 0.403 and 0.668 nm match dspacings in Bi₇O₉I₃. These results confirm that the thermal treatment leads to $Bi_7O_9I_3$ and α - Bi_5O_7I phases that are intimately mixed in the nanosized range.

The UV-visible diffuse reflectance spectra of the calcined samples showed a blue shift that depended on the temperature and length of calcination (Fig. S7). The transformation of BiOI to α-Bi₅O₇I is accompanied by a shift in the absorption edge from ~ 620 to ~ 460 nm as the color of the sample changed from dark orange to pale yellow (Fig. S8). The band gap Eg increased from 1.90 to 2.58 eV for the composites. The electronic structure was calculated by Density Function Theory using CASTEP code (Fig. S9). The valence band in BiOI is composed mainly of iodine 5p and oxygen 2p with smaller contributions from bismuth 6s and 6p orbitals while tl. conduction band is made up of bismuth 6p, iodine 5s and oxygen 2p orbitals. As the top of the valence band is derived mainly from iodine 5p orbitals, loss of iodine from BiOI w II deplete the density of states there, thus resulting in widening of the band gap.

Journal Name

3.4 Photocatalytic activity of bismuth oxylodide composites

Table 3. Physical and photocatalytic properties of calcined BiOI-pH6.

ARTICLE

Entry	BiOI (%)	Bi ₄ O ₅ I ₂ (%)	Bi ₇ O ₉ I ₃ (%)	α-Bi ₅ O ₇ I (%)	A _{BET} (m ² g ⁻¹)	E _g (eV)	C _{ads} (mg m ⁻²)	kw (h ⁻¹ g ⁻¹)	k _{SA} (h ⁻¹ m ⁻²)
as-syn	100	0	0	0	15.3	1.90	0.05	3.65	0.24
300-1	45	55	0	0	30.9	2.04	0.11	6.14	0.20
350-1	0	0	100	0	23.5	2.56	0.05	10.6	0.45
350-3	0	0	65	35	20.1	2.58	0.05	17.2	0.86
350-5	0	0	26	74	17.9	2.58	0.08	14.4	0.81
400-1	0	0	0	100	12.8	3.16	0.10	9.22	0.72

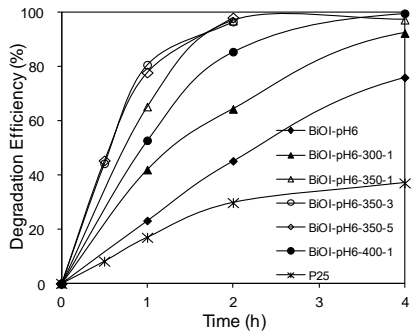


Fig. 10 Effect of calcination on photocatalytic activity of BiOI-pH6 and P25.

Compared to the as-prepared BiOI-pH6, the calcined samples showed up to fivefold higher photocatalytic activity for the degradation of p-cresol (Fig. 10). The most active photocatalysts were composites of $Bi_7O_9I_3/\alpha$ - Bi_5O_7I where > 99 % degradation efficiency was reached after only 2 h. For benchmarking, the degradation was only 37 % over P25 titania. The most active composite has a rate constant, $k_{\rm SA}$ of 0.86 h⁻¹ m-2 which is twice that of the {001}-facetted BiOI. The total organic carbon decreased from 18.7 ppm to 6.14 ppm within 2 h (Fig. S10).

The improved activity of the composites can be rationalized in terms of the energy levels of the components. The valence band energy level can be estimated according to: $E_{VB} = \chi - E^e + (\frac{1}{2})E_g$ where χ , the electronegativity of the semiconductor, is calculated as the geometric mean of the Mulliken electronegativities of the components in the semiconductor, Ee is the energy of free electrons on the hydrogen scale (taken as 4.5 eV), and Eg is the band gap of the semiconductor as determined from the onset of the optical transition (Fig. S11).³⁰ In the $Bi_7O_9I_3/\alpha$ - Bi_5O_7I system, the conduction band (CB) and valence band (VB) of Bi₇O₉I₃ are more negative than those of $\alpha\text{-Bi}_5\text{O}_7\text{I}$, thus the photogenerated electrons can transfer from the CB of Bi₇O₉I into that of $\alpha\textsc{-Bi}_5\textsc{O}_7\textsc{I}$ whereas holes can move from the VB of $\alpha\textsc{-}$ Bi₅O₇I to that of Bi₇O₉I (Fig. 11). The separation of the photoinduced electron-hole pairs at the interface of the two semiconductors increases the lifetime of the electrons and holes.

The composite $Bi_7O_9I_3/\alpha$ - Bi_5O_7I was tested for photodegradation of other phenolic compounds under visible light irradiation. Substituted phenols containing electron donating alkyl groups, such as p-cresol and 4-tert-butylphenol, were more easily degraded than phenol or 4-chlorophenol (Fig.

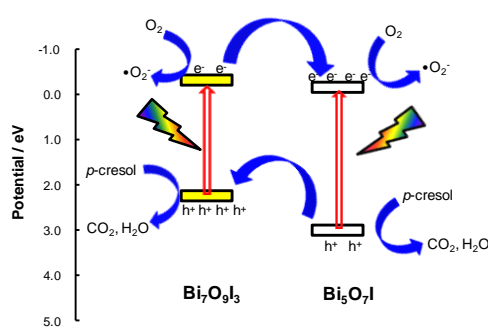


Fig. 11 Energy levels of $Bi_7O_9I_3/\alpha$ - Bi_5O_7I

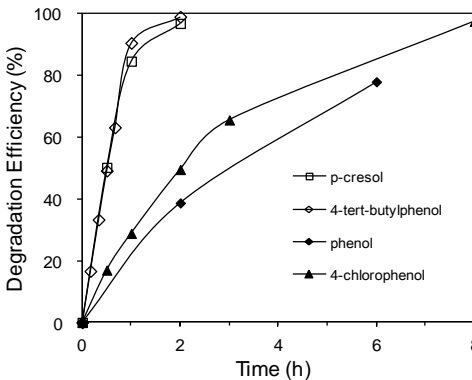


Fig. 12 Photocatalytic activity of BiOI-pH6-350-3 for phenolic compounds.

12). After 2 h, p-cresol and 4-tert-butylphenol were degraded to more than 99 % whereas the degradation efficiency was only ~ 39 % and ~ 50 % for phenol and 4-chlorophenol, respectively.

After each batch reaction, the catalyst was recovered and re-calcined at 300 °C for 2 h to remove any adsorbed organics on the surface. The recycled catalyst maintained its photodegradative activity for p-cresol even after four runs (Fig. S12a). The x-ray diffractograms of the fresh and recycled catalysts showed no significant difference (Fig. S12b), indicating its stability and reuseability. Additionally, we al examined the photoactivity in the presence of coexisting ions, which are common in wastewater (Fig. S13). The sample BiOIpH6-350-3 maintained its activity in the presence of 1 mmol L NO₃ and even had a slightly higher activity in the presence of Cl⁻. These results support the potential usage of the materi for wastewater treatment.

Journal Name

3.5 Active species

In order to gain some insight into the active species involved in the photodegradation of p-cresol over $Bi_7O_9I_3/\alpha$ - Bi_5O_7I , radical scavengers and N2 and O2 purging were used. The presence of the •OH radical can be detected by its reaction with terephthalic acid to produce 2-hydroxyterephthalic acid which fluoresces at 425 nm.31 However, there was no obvious increase in the peak intensity at 425 nm even after 2 h of irradiation (Fig. S14), indicating that no •OH radicals were formed for the $Bi_7O_9I_3/\alpha$ - Bi_5O_7I composite. Addition of excess tert-butanol, a known •OH scavenger, 32 also did not affect the degradation efficiency (Table 4). The participation of holes was tested by adding a hole scavenger, K₂C₂O₄, to the photoreaction system.³³ The rate constant dropped drastically to only 7 % of that without the scavenger, suggesting that holes play a major role in the degradation of p-cresol.

Table 4. Photodegradation of p-cresol over $Bi_7O_9I_3/\alpha$ - Bi_5O_7I in the presence of various scavengers and gas atmosphere.

Scavenger	Purging gas	Amt (µmol)	k (h ⁻¹ g ⁻¹)	Radical tested
-	-	-	17.2	-
-	N_2	-	7.20	•O2 ⁻
-	O_2	-	27.9	•O2 ⁻
t-butanol	-	110	16.1	•OH
$K_2C_2O_4$	-	110	1.19	holes
KBrO₃	-	110	122	•O2 ⁻
$KBrO_3(N_2)$	-	110	127	•O2 ⁻
KBrO ₃	-	44	102	•O2 ⁻

Purging the reaction system with nitrogen to remove any dissolved oxygen led to lower degradation efficiency. In contrast, the reaction rate was increased over that at ambient conditions when oxygen was bubbled into the solution, showing that the presence of oxygen is important. The dissolved oxygen can react with photoinduced electrons to form the superoxide radical ${ullet} O_2^-$ or it can act only as an electron acceptor to reduce the electron-hole recombination. To clarify the role of oxygen, KBrO₃ was added to the reaction system with and without nitrogen purging. Potassium bromate, a strong oxidant, is known to be a good electron acceptor and can be reduced as follows: 34,35

$$BrO_3^- + e^- + 2H^+ \rightarrow BrO_2 + H_2O$$

$$BrO_3^- + 6e^- + 6H^+ \rightarrow [BrO_2^-, HOBr] \rightarrow Br^- + 3H_2O$$

Its addition should reduce the electron-hole recombination in the photocatalyst, thus increasing the quantum efficiency without producing superoxide radicals. The reaction was ~ 7 times faster after adding KBrO₃ which can be attributed to the decrease of electron-hole recombination. The reaction rate remained high and was unaffected by nitrogen purging, indicating that superoxide radicals are not involved in the degradation process. Rather, the addition of KBrO₃ effectively suppressed the recombination of photo-generated holes with electrons resulting in the enhanced activity. This result lends further support that holes are the main species for the photodegradation of *p*-cresol over $Bi_7O_9I_3/\alpha$ - Bi_5O_7I .

Intermediates formed during photodegradation of p-cresol 1 were identified using LC-MS (Fig. S15). Several intermediated could be detected. Oxidation of the methyl group in p-cresol leads to 4-hydroxybenzyl alcohol 2 which undergoes further reaction to 4-hydroxybenzaldehyde 4 and 4-hydroxybenzcic acid 6. Dimerization of 4-hydroxybenzyl radical gives 4-(4hydroxy phenethyl)phenol 7. Its formation has been attributed to the relatively long lifetime of the 4-hydroxybenzyl radical intermediate, which increases the probability dimerization.³⁶ Besides oxidation at the methyl group, products due to the benzene ring oxidation such as 4-methyl benzene diols 3 and dihydroxy benzaldehydes 5 were also detected. Mineralization of the intermediates into CO2 and H₂O was confirmed by the decrease in the TOC upon photoirradiation.

Scheme 1. Proposed degradation pathway of p-cresol over BiOI-pH6-350-3.

4. Conclusions

Single crystalline nanosheets of BiOI with either predominantly {001}- or {110}-exposed facets were obtained by varying the pH during hydrothermal synthesis. Under acidic conditions (pH 2.3 – 4), the {001} facets were preferentially formed while BiOl with {110} dominant facets was formed at pH 5 to 8. The surface area of BiOI increased with increasing synthesis pH due to the formation of smaller and thinner nanosheets. The intrinsic photoactivity for p-cresol degradation under visible light irradiation of the {001}-facetted BiOI was about twice that of BiOI with {110} exposed facets when compared on unit surface area. Calcination of the {110}-facetted BiOI led to tl replacement of some of the iodine by oxygen. The heterojunctioned Bi_xO_vI_z composites formed by this process showed better photocatalytic activity than BiOI. A Bi₇O₉I₃/ .- Bi_5O_7I composite had the highest photocatalytic activity for pcresol and other phenolic compounds. Experiments wi'. various scavengers and under aerobic and anaerob

ARTICLE Journal Name

conditions point to holes as the species responsible for most of the photodegradation.

Acknowledgement

Financial support from the National Research Foundation and the Economic Development Board (SPORE, COY-15-EWI-RCFSA/N197-1) for a research assistantship for A. Han and a research scholarship for J. Sun is gratefully acknowledged. The work is supported by the Ministry of Education ARC Tier 1 grants R-143-000-550-112 and R-143-000-603-112.

References

- R. Asahi, T. Morikawa, T. Ohwaki, K. Aoki and Y. Taga, Science, 2001, 293, 269-271.
- 2 J. G. Yu, Y. R. Su and B. Cheng, Adv. Funct. Mater., 2007, 17, 1984-1990.
- Z. Zhang, C. C. Wang, R. Zakaria and J. Y. Ying, J. Phys. Chem. B, 1998, 102, 10871-10878.
- 4 W. Chen, Q. Kuang, Q. Wang and Z. Xie, RSC adv., 2015, 5, 20396-20409.
- 5 J. N. Wilson and H. Idriss, J. Am. Chem. Soc. 2002, 124, 11284-11285.
- 6 M. Lazzeri, A. Vittadini and A. Selloni, Phys. Rev. B: Condens. Matter Mater. Phys., 2001, 63, 155409.
- 7 J. Jiang, K. Zhao, X. Xiao and L. S. Zhang, J. Am. Chem. Soc., 2012, 134, 4473-4476.
- 8 R. Li, F. Zhang, D. Wang, J. Yang, M. Li, J. Zhu, X. Zhou, H. Han and C. Li, *Nat. Commun.*, 2013, 4, 1432.
- 9 Y. Yang, G. Wang, Q. Deng, H. Wang, Y. Zhang, D. H. L. Ng and H. Zhao, RSC adv., 2014, 4, 34577-34583.
- 10 Y. Bi, S. Ouyang, N. Umezawa, J. Cao and J. Ye, J. Am. Chem. Soc., 2011, 133, 6490-6492.
- 11 J. Miao and B. Liu, RSC Adv., 2013, 3, 1222-1226.
- 12 H. Zhang, Lu. Liu and Z. Zhou, RSC Adv., 2012, 2, 9224-9229.
- 13 J. Henle, P. Simon, A. Frenzel, S. Scholz and S. Kaskel, *Chem. Mater.*, 2007, **19**, 366-373.
- 14 Z. Liu, W. Xu, J. Fang, X. Xu, S. Wu, X. Zhu and Z. Chen, Appl. Surf. Sci., 2012, 259, 441-447.
- 15 P. Q. Wang, Y. Bai, J. Y. Liu, Z. Fan and Y. Q. Hu, *Micro Nano Lett.*, 2013, 8, 99-101.
- 16 Y. Wang, K. Deng and L. Zhang, *J. Phys. Chem. C*, 2011, **115**, 14300-14308.
- 17 X. Chang, J. Huang, Q. Tan, M. Wang, G. Ji, S. Deng S and G. Yu, Catal. Commun., 2009, 10, 1957-1961.
- 18 R. Hao, X. Xiao, X. Zuo, J. Nan and W. Zhang, J. Hazard. Mater., 2012, 209–210, 137-145.
- 19 X. Wang, S. Yang, H. Li, W. Zhao, C. Sun and H. He, RSC Adv., 2014, 4, 42530-42537.
- 20 X. Xiao and W. Zhang, J. Mater. Chem., 2010, 20, 5866-5870.
- 21 J. Liu, H. Li, N. Du, S. Song and W. Hou, RSC. Adv., 2014, 4, 31393-31399.
- 22 L. Ye, L. Tian, T. Peng and L. Zan, J. Mater. Chem., 2011, 21, 12479-12484.
- 23 E. Keller and V. Krämer, Acta Crystallogr., Sect. C: Cryst. Struct. Commun., 2007, C63, i109-i111.
- 24 P. Rittner and H. Oppermann, Z. Anorg. Allg. Chem., 1992, 617, 131-135.
- 25 M. Schmidt, H. Oppermann, H. Brückner and M. Binnewies, Z. Anorg. Allg. Chem., 1997, 623, 1945-1953.
- 26 E. Keller, V. Krämer, M. Schmidt and H. Oppermann, Z. Kristallogr. Cryst. Mater., 2002, 217, 256-264.
- 27 U. Eggenweiler, J. Ketterer, E. Keller and V. Krämer, Z. Kristallogr. Cryst. Mater., 2001, 216, 230-233.

- 28 J. Ketterer, E. Keller and V. Krämer, Z. Kristallogr. Cryst. Mater., 1985, 172, 63-70.
- 29 R. A. Smith, Semiconductors, 2nd ed., Cambridge University Press, Cambridge, U.K., 1978.
- 30 M. A. Butler and D. S. Ginley, *J. Electrochem. Soc.*, 1978, **125**, 228-232.
- 31 C. Karunakaran and P. Anilkumar, J. Mol. Catal. A: Chem., 2007, 265, 153-158.
- 32 J. Ma, and N. J. D. Graham, Water Res., 2000, 34, 3822-3828.
- 33 A. J. Hoffman, E. R. Carraway and M. R. Hoffmann, *Environ. Sci. Technol.*, 1994, **28**, 776-785.
- 34 S. Qourzal, N. Barka, M. Tamimi, A. Assabbane and Y. Ait Ichou, Appl. Catal., A, 2008, 334, 386-393.
- 35 W. Bahnemann, M. Muneer and M. M. Haque, Catal. Today, 2007, 124, 133-148.
- 36 A. Mylonas and E. Papaconstantinou, *Polyhedron*, 1996, **15**, 3211-3217.